Turkish Journal of Earth Sciences

Volume 34
Number 2 *SI-1*

Article 8

2-20-2025

Multianalytical characterization of Byzantine wall paintings by SEM-EDX,μ-XRD, raman and FTIR techniques

ONUR ŞİMŞEK

FATİH ÖZBAŞ

ERSİN KAYGISIZ

GÖZEM YAŞAYAN

GÜLCE ÖĞRÜÇ ILDIZ

Recommended Citation

ŞİMŞEK, ONUR; ÖZBAŞ, FATİH; KAYGISIZ, ERSİN; YAŞAYAN, GÖZEM; and ILDIZ, GÜLCE ÖĞRÜÇ (2025) "Multianalytical characterization of Byzantine wall paintings by SEM-EDX,μ-XRD, raman and FTIR techniques," *Turkish Journal of Earth Sciences*: Vol. 34: No. 2, Article 8. https://doi.org/10.55730/1300-0985.1957

Available at: https://journals.tubitak.gov.tr/earth/vol34/iss2/8

TÜBİTAK

Turkish Journal of Earth Sciences

http://journals.tubitak.gov.tr/earth/

Research Article

Turkish J Earth Sci
(2025) 34: 246-262

doi:10.55730/1300-0985.1957

Multianalytical characterization of Byzantine wall paintings by SEM-EDX, μ-XRD, raman and FTIR techniques

Onur ŞİMŞEK[1,*], Fatih ÖZBAŞ[1,2], Ersin KAYGISIZ[2,3], Gözem YAŞAYAN[2], Gülce Öğrüç ILDIZ[4]

[1]Department of Architecture, Faculty of Art, Design and Architecture, Fatih Sultan Mehmet Vakıf University, İstanbul, Turkiye
[2]Research Center for the Conservation of Cultural Property of Foundation, Fatih Sultan Mehmet Vakif University, İstanbul, Turkiye
[3]Department of Geological Engineering, Faculty of Engineering, Istanbul University-Cerrahpasa, İstanbul, Turkiye
[4]Department of Physics, Faculty of Sciences and Letters, İstanbul Kültür University, İstanbul, Turkiye

Received: 19.06.2024 • **Accepted/Published Online:** 10.12.2024 • **Final Version:** 20.02.2025

Abstract: In this study, various analytical methods were employed to examine the mineral based natural pigments in the frescoes of the medieval (9th century) Byzantine church, known today as the Atik Mustafa Pasha Mosque. The techniques include μ-X-ray diffraction (μ-XRD), Raman and Fourier transform infrared (FTIR) spectroscopies, and scanning electron microscopy coupled with energy dispersive X-ray spectroscopy (SEM–EDX). The SEM-EDX technique enabled the identification of the chemical element composition in the studied pieces, while Raman and FTIR spectroscopies, as well as XRD, allowed the identification of mineral phases and mineral based natural pigments in the paints of the frescoes. Fragments of various colors (red, black, yellow, green, pink, cream, and white) were investigated. The analyses showed that the red (and pink) tones were primarily due to hematite (Fe_2O_3), goethite (FeO(OH) and cinnabar (HgS), amorphous carbon (C) was used to achieve the black color. Yellow tones were mostly attributed to limonite ($FeO(OH)\cdot nH_2O$) and the greens were the result of celadonite ($K(Mg,Fe^{2+})(Fe^{3+},Al)[Si_4O_{10}](OH)_2$), while the white color was provided by calcite. The combined application of the different analytical methods used proved to be a powerful tool for identifying and determining the compositional makeup of the mineral based natural pigments present in the studied samples. This highlights the importance of a multi-analytical approach in characterizing the investigated historical wall paintings.

Key words: Byzantine wall paintings, mineral based natural pigments, cultural heritage, μ-XRD, Raman, FTIR

1. Introduction

The aim of this study was to investigate the original wall painting mineral based natural pigments used in the frescoes of the mid-9th century Byzantine period church; latter converted into a mosque in the early 16th century. Different characterization methods were employed to identify the mineral based natural pigments and determine their chemical composition (micro-X-ray diffraction analysis (μ-XRD), Raman and Fourier transform infrared (FTIR) spectroscopies, and scanning electron microscopy coupled with energy dispersive X-ray spectroscopy (SEM–EDX)). The goal is for restorers to utilize the data obtained in the present investigation of the frescoes belonging to the original structure during the restoration works of the mosque, specifically in the subsequent cleaning, repairing, and preservation processes.

The church is believed to have originally served as the central element of a monastery and was constructed as one of the first cross-in-square churches, featuring a central dome and three apses on the east side - an architectural plan that was most used for churches during the middle Byzantine period (Demus, 1964). It is considered that on its North and South sides, there were side chapels (parekklesion). Nevertheless, the origins of the church are still under debate. According to the architectural elements used in the building, the first construction dates from the second half of the 9th century, sharing similarities with other churches from the period of Emperor Theophilos. It has been suggested that Thecla, the daughter of Theophilos, ordered the building of the church in honor of St. Thecla (Eyice, 1991a; Wiener Müller-Wolfgang, 2001). However, other names, such as Sts. Peter and Mark, Sts. Cosmas and Damianos, and St. Elias of Petrion, have also been suggested by historians (Encyclopedia of the Hellenic World, 2023).

Nowadays called Atik Mustafa Pasha Mosque[1], after the Ottoman grand vizier Koca Mustafa Pasha, the building is

[1]The Atik Mustafa Pasha Mosque is also known as *Hazreti Jabir Mosque*, because it is believed that Jabir bin Abdullah, a companion of the Prophet, is entombed in the south-eastern corner of the *bema* part (Esmer, 2016).

* Correspondence: osimsek@fsm.edu.tr

located next to the Golden Horn in the modern İstanbul Fatih/Ayvansaray district (Figure 1) (Yandex Maps; Google Earth Website) a vibrant and culturally diverse urban quarter in the northwest corner of the Historic Peninsula of Istanbul. During the Byzantine period, this area was known as Blakhernae, and it was the location of the Blakhernae Palace (Esmer, 2016). This district belonged to the XIV Regio as part of the historical center of Constantinople, after the Byzantine Emperor Manuel Komnenos enlarged the borders of the city (Eyice, 1991b).

This church was one of the two that have been converted by Koca Mustafa Pasha into a mosque. To differentiate between the two mosques, the adjective "atik" (old) was added to the name of this one. For its new purpose as a mosque, several modifications were applied. These include the construction of a mihrab, marking the position of the imam, which is located within the central eastern apse of the building and is crowned by a conch (half-dome) (Figure 1e) (Kızılkayak, 2023). The original Byzantine cupola with windows was replaced by an Ottoman dome, new windows and a minaret were added, and some of the original windows were closed by brick or stone. The roof underwent extensive renovation, and on the western facade a last prayer area with five marble columns was added, following the traditional mosque building scheme. From the Byzantine period, the barrel vaults above the central cross remained.

The building was damaged by a fire in 1729, and the earthquake of 1894 destroyed the minaret, among other elements. In 1906, during the rule of Abdulhamid II, the minaret was reconstructed. On the south facade, frescoes of St. Kosmas, Archangel Michael, and St. Damianos, dating from the 14th or 15th century, remained above the windows (Figure 1c) (Kızılkayak, 2023). During the restoration undertaken in 1956, these frescoes were discovered and subsequently hidden behind wood (Mathews and Ernest, 1985). The same frescoes were covered by plaster during the restoration undertaken in 1992.

The current restoration of the mosque started in 2021 and has been highlighting the architectural and historical significance of this mosque and of its decorative elements (Figure 1d, Figure 1e). During the restoration, the original ground floor level was discovered, revealing rich mosaic decorations (Figure 1g). It was revealed that during the Ottoman period, the floor level of the building was elevated more than 1 meter above the original ground level of the church (Figure 1f). Details at the lower wall level have revealed that originally colored marble plates were covering the walls. However, the marble plates were later removed and replaced by fresco paintings, still during the Byzantine period. Unique fresco examples, featuring ornaments or scenes of wrongdoers in the afterlife, were found between the floor level of the Ottoman Mosque and the original floor level of the former Byzantine church. These frescoes are significant for the Byzantine art history in Türkiye, because they are the first examples of this type from the middle Byzantine period in Istanbul. The mosque is expected to be reopened by late 2023 after the ongoing restoration (Türkyılmaz, 2023).

The identification of mineral based natural pigments used in cultural heritage artifacts is crucial for their restoration, preservation, dating, and authentication (Bell et al., 1997; Edwards et al., 2000; Smith and Clark, 2004). Frescoes are common artworks on the walls of old churches, spread over a wide geographical area. Especially in recent years, the investigation of Roman wall painting techniques and the mineral based natural pigments used, through modern analytical methods, has been gaining relevance. Nevertheless, in Türkiye, despite several known examples (Akyol et al., 2005; Dooryhée et al., 2005; Akyuz et al., 2009; Weber et al., 2009; Akyol et al., 2011; Zimmermann, 2011; Bakiler et al., 2016), this type of study is still relatively scarce. In the literature, Fikri et al. (2022) utilized ATR-FTIR, XRF and Raman techniques for characterizing wall paintings in Morocco (North Africa) (Fikri et al., 2022). Koochakzaei et al. (2022) highlighted the importance of SEM-EDS, micro-Raman, and FTIR techniques for mineral based natural pigment analysis in wall paintings in Isfahan, Iran (Asia) (Koochakzaei et al., 2022). In another study, Marrocchino et al. (2022) reported the role of SEM-EDS, micro-Raman, and XRF techniques in analyzing mineral based natural pigments in wall paintings in Certosa di Calci, Pisa in Italy (Europe) (Marrocchino et al., 2022). Colored components of murals in cultural heritage artifacts are nowadays investigated using various analytical techniques, such as Raman and FTIR spectroscopies (Crupi et al., 2015; Piovesan et al., 2016; Barone et al., 2018; Germinario et al., 2018), XRD (Mazzocchin et al., 2004; Uvarov et al., 2015; Bakiler et al., 2016) and SEM-EDX (Uvarov et al., 2015; Bakiler et al., 2016). Due to the potential damage caused by certain methods, samples were extracted from sections of the building that had fallen or broken off naturally and were subsequently analyzed. Considering the historical significance and distinctive nature of these samples, it is evident that cultural heritage objects necessitate special care during the analysis process.

The application of spectroscopic analyses to cultural heritage objects has a long history, starting in the 1950s, and mineral based natural pigments have since always been among the preferred elements for analysis (Olin, 1966; Van't Hul-Ehrnreich, 1970; Gilbert et al., 2003; Franquelo et al., 2009). FTIR and Raman spectroscopies provide detailed molecular information, and they have gained a prominent role over the years as very powerful techniques for the investigation of mineral based natural

Figure 1. a) and b)[2] Map of the location of the Atik Mustafa Pasha Mosque; c) and d) Overview of the mosque before and during restoration; e) A view of the dome, mihrab, minbar, and decorative patterns inside the mosque before restoration; f) Image showing the floor level of the mosque (marked with a red line), raised more than 1 m above the original floor level of the church during the Ottoman period; g) Mosaic decoration of the original ground floor of the Byzantine church.

[2]Yandex Maps, (2023). URL https://yandex.com.tr/harita/?ll=28.247374%2C40.823802&z=8.07 (accessed 08.30.24).

pigments, either organic or inorganic, natural, or synthetic, often used in combination with XRD, which is also a highly effective method for materials characterization. When combined with techniques that afford elemental composition, such as the SEM-EDX method (Zeng et al., 2010; Tomasini et al., 2012; Rosado et al., 2013; Mahmoud, 2014). FTIR, Raman and XRD can provide a detailed chemical characterization of the materials under study. The combined use of these techniques is then taken advantage in the present investigation, highlighting the importance of a multianalytic approach in the characterization of the investigated historical wall paintings.

2. Materials and methods

The samples used in this study are from the original church's frescoes and were obtained with the permission of the T.R. Directorate General of Foundations before the commencement of the mosque's current restoration in 2021. Black, green, red, yellow, pink, white and cream-colored plaster samples were taken from the wall paintings (6 samples), specifically from the locations indicated in Figure 2. Microscopic images were taken to closely examine the morphology and texture of the samples prior to Raman, FTIR, and μ-XRD analyses, and these images are shown in Figure 3.

The morphology of the samples was examined using the Nikon SMZ 745T stereomicroscope and the Zeiss Axio Imager A2m, both located within the Research Center for the Conservation of Cultural Property of Foundation, Fatih Sultan Mehmet Vakıf University. The elemental compositions of the paintings were determined using a SEM/Hitachi SU3500 equipped with an EDX micro-analytical system (Oxford X-ACT) at the Aluminum Testing Training and Research Center at Fatih Sultan Mehmet Vakif University, utilizing a 30 kV electron beam under low vacuum. No coating was applied to prevent charge effects. The EDX analyses were performed on fourteen representative samples exhibiting different colors.

μ-XRD patterns were collected at room temperature using a Bruker D8 Discover diffractometer equipped with a Vantec 500 detector at the Material Research Center for Cultural Property and Artworks of Mimar Sinan Fine Arts

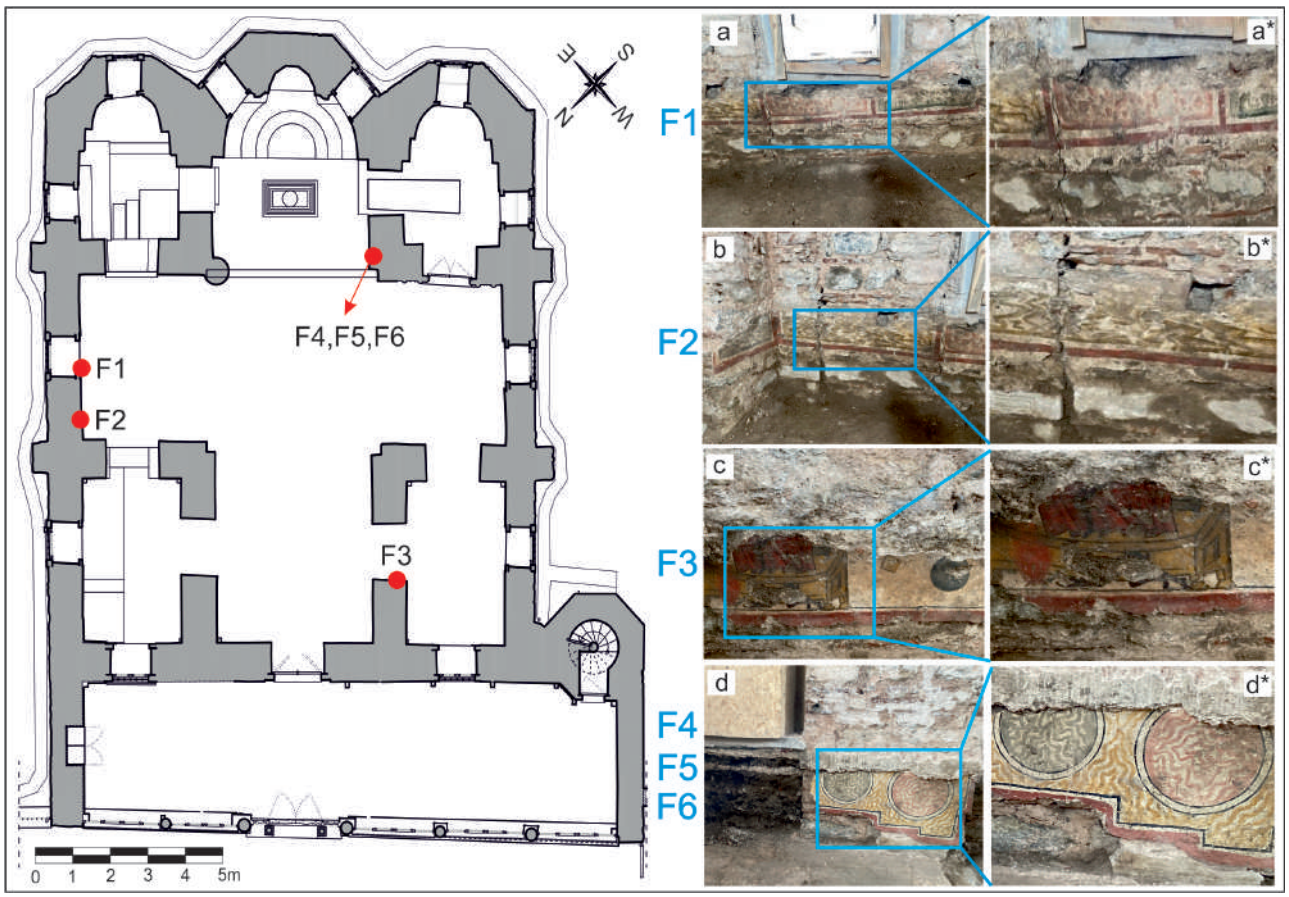

Figure 2. General plan of the mosque, showing the places from where the samples were taken (red dots) (left), and far (Figures 2a–2d) and near (Figures 2a*–2d*) views of the walls from which the samples were taken.

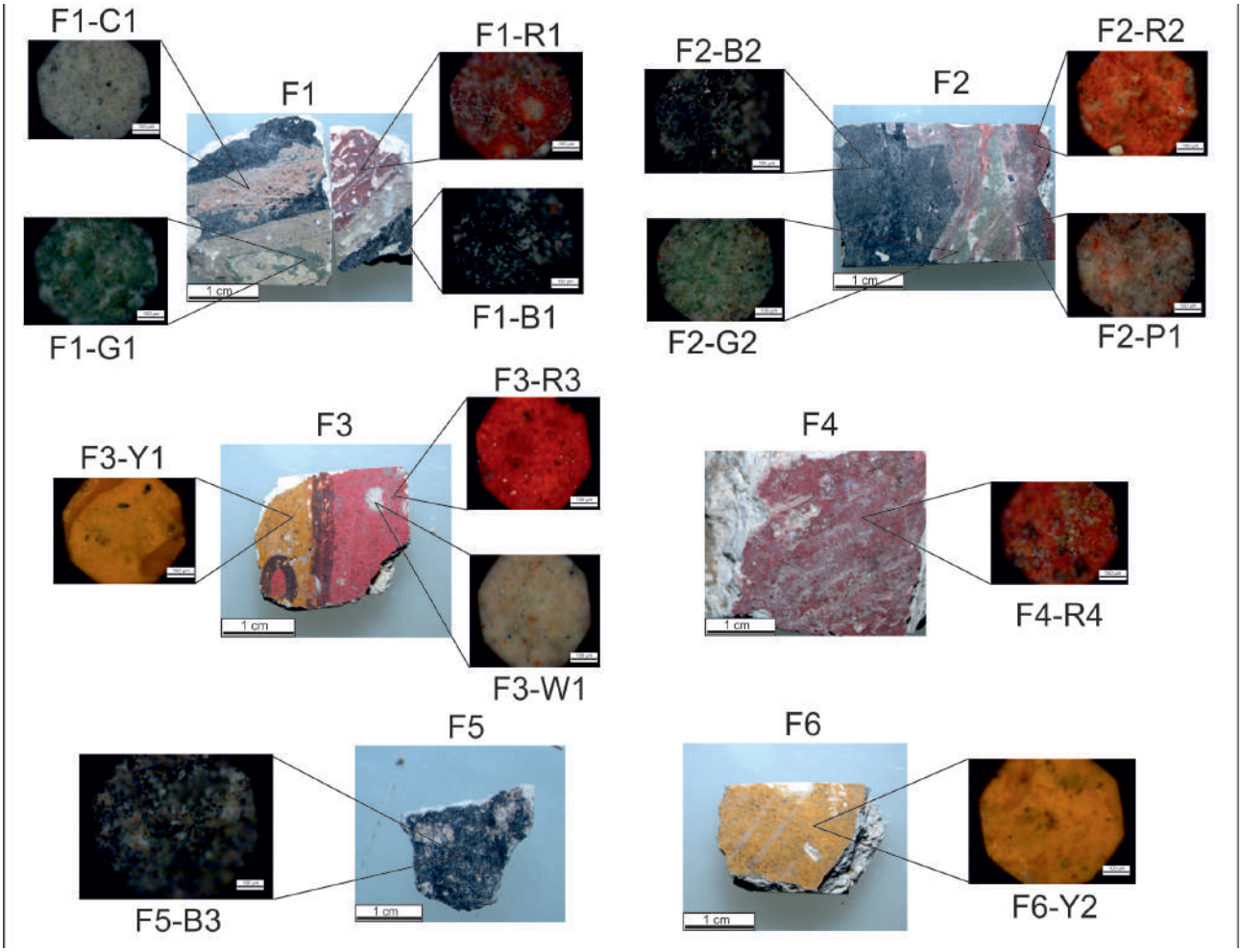

Figure 3. Stereo microscope images of the samples used in the study (R: red, B: black, G: green, P: pink, Y: yellow, C: cream, and W: white) (in large images, the scale is 1 cm, while in the detailed smaller images, the scale is 100 μm).

University, with a goniometer speed of 2θ = 1°/min and Cu Kα radiation (λ = 1.5418 Å; 40 kV; 30 mA). For data collection, a 2q scan range between 5° and 80° was used, with a step size of 0.02°, a divergence slit of 0.5 mm and a receiving slit of 0.3 mm. A Cu anode was used during the analyses. No fluorescence effects were observed in the XRD patterns. All measurements were made from the surface of the samples, using a 0.5 mm collimator. The analyses of the XRD patterns (phase identification) were performed using the Philips X'Pert High Score Plus software (PDF-2 Release 2003) package in conjunction with the Joint Committee on Powder Diffraction Standards (JCPDS) database.

The Raman spectra of the different colored regions of the collected samples were obtained using a multichannel Renishaw inVia spectrometer equipped with a Peltier-cooled CCD detector at the Nanotechnology Application and Research Center of İstanbul Technical University. A diode laser (785 nm) was used as excitation source (System operating with laser wavelengths in the range 320 nm to 1064 nm and power consumption:150W). Different laser powers ranging from 1% to 5% were used for Raman analysis of samples with various colors. Samples were scanned in the wavenumber range of 100 to 2000 cm^{-1} and with a spectral resolution of 2 cm^{-1}. To provide a better signal-to-noise ratio, the integration time was set as 10 s, and 5–10 scans were coadded to generate the final spectra. For each sample, the analyses were repeated in different spots.

The IR spectra were obtained in ATR mode using a Jasco-6800 FTIR spectrometer equipped with a diamond single-bounce ATR accessory and Spectra Manager software at the Research Center for the Conservation of Cultural Property of Fatih Sultan Mehmet Vakıf University. Thirty-two scans were co-added, with a 4 cm^{-1} resolution, in the spectral range of 4000–400 cm^{-1}. The spectrum of air was used as the background in the measurements.

3. Results

3.1. SEM-EDX

SEM-EDX analyses were performed on the differently colored regions of the samples. The results are shown in Table 1.

The SEM-EDX analyses of the red samples (see Table 1, and also Figure 3, for sample identification) showed the presence of sulfur (S) and calcium (Ca) as major constituents (with mercury in sample F3-R3), silicon (Si), iron (Fe), and aluminum (Al), as main minor components. Sulfur and calcium were also detected as major elements in the black, pink, cream, and green samples (with residual sulfur in F5-B3), while in the yellow and white samples, sulfur was present in considerably lower amounts, with calcium being the sole major constituting element. Silicon was observed in significant amounts in the yellow, pink, and white samples, while aluminum and iron appeared in their maximum amounts in the yellow samples (iron was also found to be present in large amounts in one of the red samples, F2-R2). Minor amounts of sodium, potassium, magnesium and phosphorous were also determined in most of the studied samples.

3.2. µ-XRD

The µ-XRD results presented in Table 2, specifying the minerals identified in the different samples. The diffractograms for each sample are shown in Figures 4–7. In the XRD analyses, diffractograms were obtained from crystals at the surface of the samples with different orientations, and the samples presented different degrees of crystallization. As a result, the intensities of the signals vary from sample to sample, necessitating the use of different reference data values for the same mineral in the analyses.

3.3. Raman and IR spectroscopy

The minerals/ mineral based natural pigments identified by Raman and IR spectroscopies, along with their characteristic Raman reference bands and references, are listed in Table 3. The spectra are shown in Figures 8– 11.

4. Discussion

4.1. Red samples

The SEM-EDX analyses of the red samples F1-R1 and F2-R2 revealed the dominant presence of sulfur and calcium in these samples, with iron being also present in large amount in F2-R2. The F3-R3 sample has a large content of mercury, and F4-R4 has calcium and iron as major constituting elements (Table 1). All samples show significant amounts of silicon and aluminum. These results agree with those obtained by µ-XRD and Raman/ IR spectroscopies, which demonstrated that in the F1-R1 sample was totally gypsum and F2-R2 sample, the major constituting minerals were gypsum ($Ca(SO_4).2H_2O$), calcite (Ca. 7–8%, $CaCO_3$) and hematite (Fe_2O_3). Hematite is responsible for the red color of these samples. On the other hand, F3-R3 (mainly gypsum) owes its color to the presence of cinnabar (HgS), a well-known red mineral based natural pigment in antiquity, along with a small amount of limonite $FeO(OH)\cdot nH_2O$, which is frequently

Table 1. SEM-EDX results of the bulk samples in the differently colored areas (values in %).

Element Oxide	F1-R1	F2-R2	F3-R3	F4-R4	F1-B1	F2-B2	F5-B3	F1-G1	F2-G2	F3-Y1	F6-Y2	F1-C1	F2-P1	F3-W1
CaO	40.95	37.45	38.17	82.89	41.76	44.18	88.17	48.77	40.75	60.41	73.12	41.46	42.27	71.97
SO_3	46.96	35.34	14.73	ND	50.59	38.04	0.76	39.13	43.59	9.48	ND	52.14	32.30	8.62
SiO_2	5.17	6.72	6.00	6.33	4.13	8.61	3.24	6.25	7.51	13.59	13.04	2.86	12.40	10.35
Al_2O_3	1.90	2.51	2.79	2.93	1.08	3.18	3.78	1.55	2.00	6.73	7.16	1.19	4.77	4.47
MgO	0.72	1.71	ND	0.79	0.63	1.83	1.20	0.63	0.98	1.26	0.56	0.44	2.68	0.84
FeO	2.90	13.64	1.79	6.22	0.69	1.57	ND	2.04	1.95	6.58	6.12	0.50	2.92	1.77
Na_2O	0.78	1.17	0.84	0.84	0.52	1.00	1.25	ND	ND	0.69	ND	0.59	1.36	0.74
K_2O	ND	ND	ND	ND	ND	ND	ND	0.98	1.18	ND	ND	ND	ND	ND
HgO	ND	ND	35.67	ND	ND	ND	ND	ND	ND	ND	ND	ND	ND	ND
P_2O_5	ND	ND	ND	ND	ND	ND	0.52	ND	ND	0.87	ND	ND	ND	0.88

ND: not detected.

Table 2. Summary of μ-XRD results.

Reference Code	Mineral Name	F1-R1	F2-R2	F3-R3	F4-R4	F1-B1	F2-B2	F5-B3	F1-G1	F2-G2	F3-Y1	F6-Y2	F1-C1	F2-P1	F3-W1
01-086-2339	Calcite	+				+	+		+				+		
01-072-1937			+	+	+			+		+	+	+		+	+
00-033-0311	Gypsum			+											+
00-036-0432		+	+		+	+	+		+	+		+	+	+	
01-085-0987	Hematite		+								+			+	
00-024-0072		+			+										
01-074-2195	Limonite/ Goethite			+							+	+			
00-003-0427	Quartz					+							+		
00-042-1408	Cinnabar			+											+
01-083-2008	Celadonite								+	+					

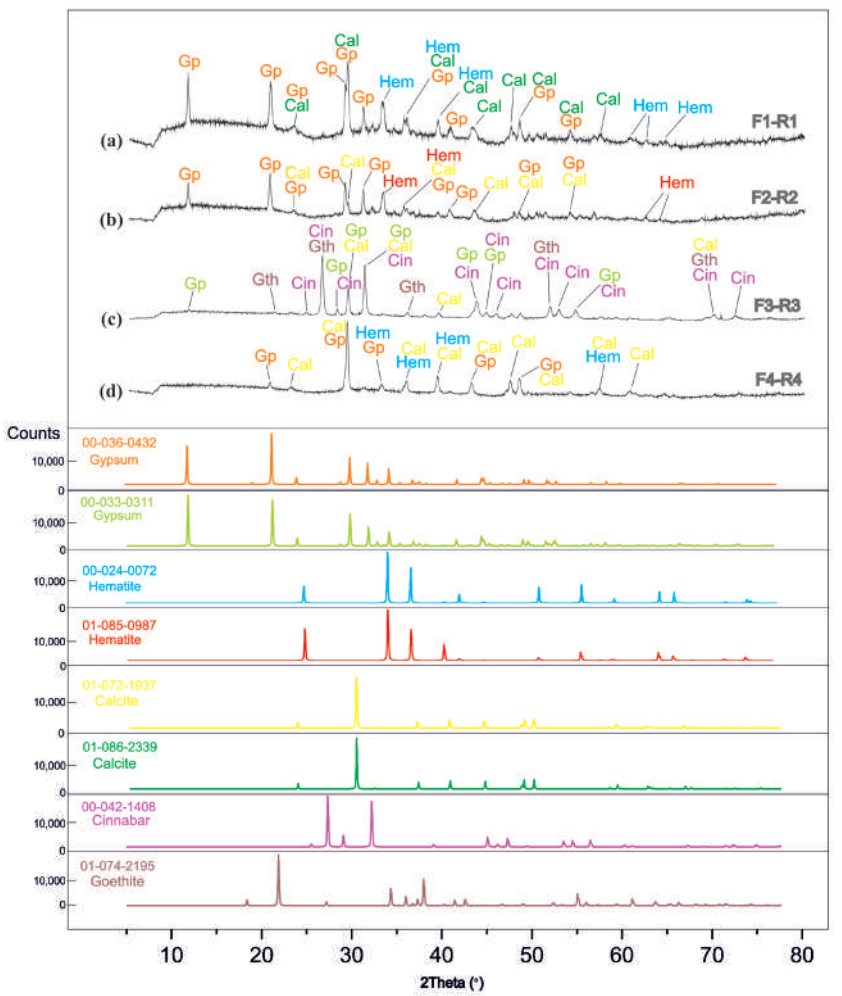

Figure 4. μ-X-ray diffraction pattern of the bulk red samples' surface. Identified minerals: calcite (Cal), gypsum (Gp), hematite (Hem), goethite (Gth), quartz (Qz), cinnabar (Cin).

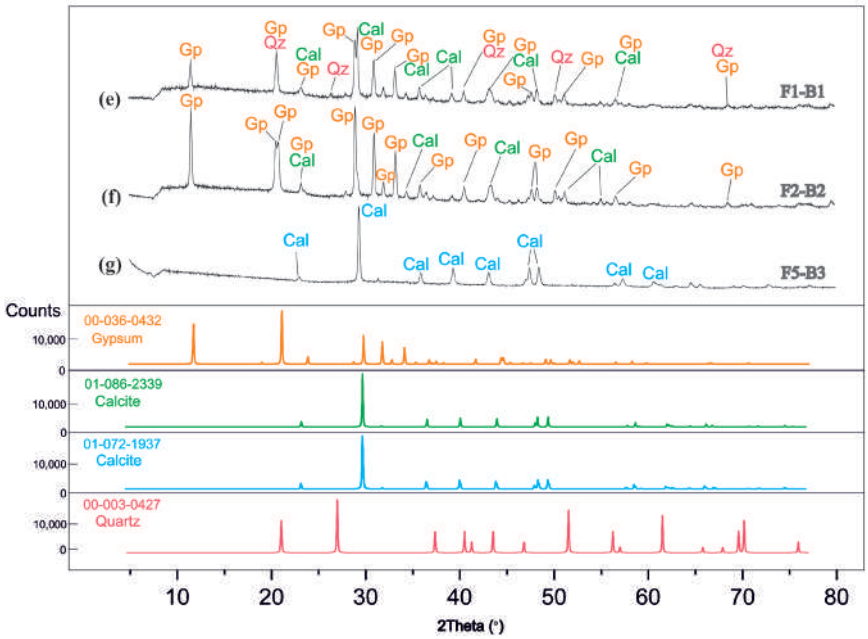

Figure 5. µ-X-ray diffraction pattern of the bulk black samples' surface. Identified minerals: calcite (Cal), gypsum (Gp), quartz (Qz).

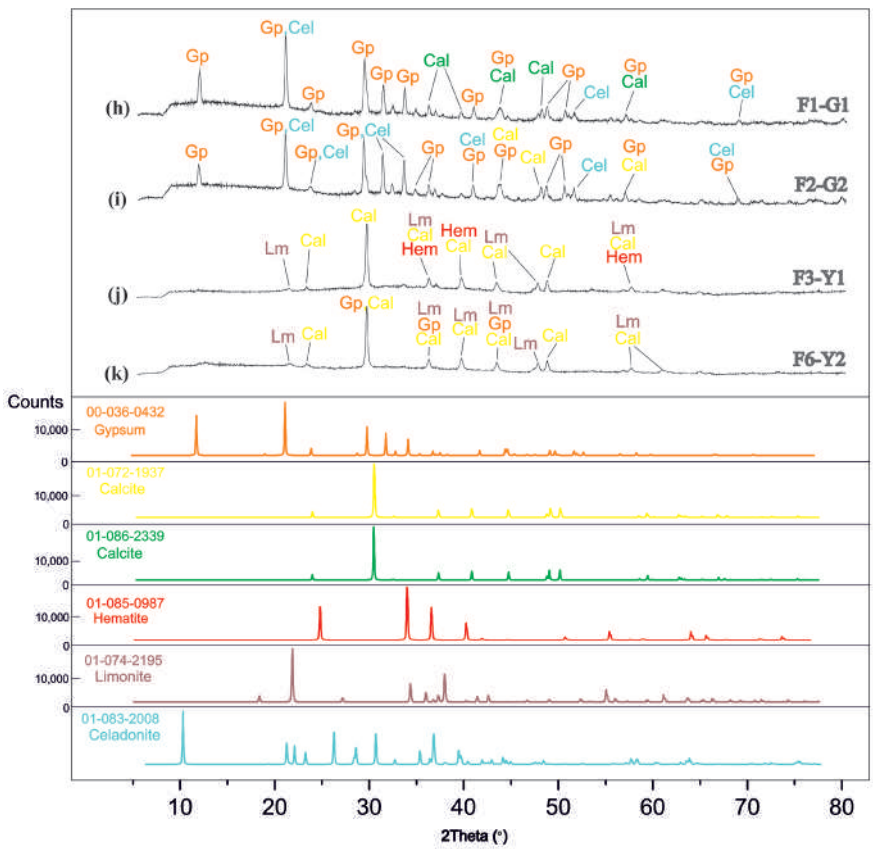

Figure 6. µ-X-ray diffraction pattern of the bulk green and yellow samples' surface. Identified minerals: calcite (Cal), gypsum (Gp), hematite (Hem), limonite (Lm), celadonite (Cel).

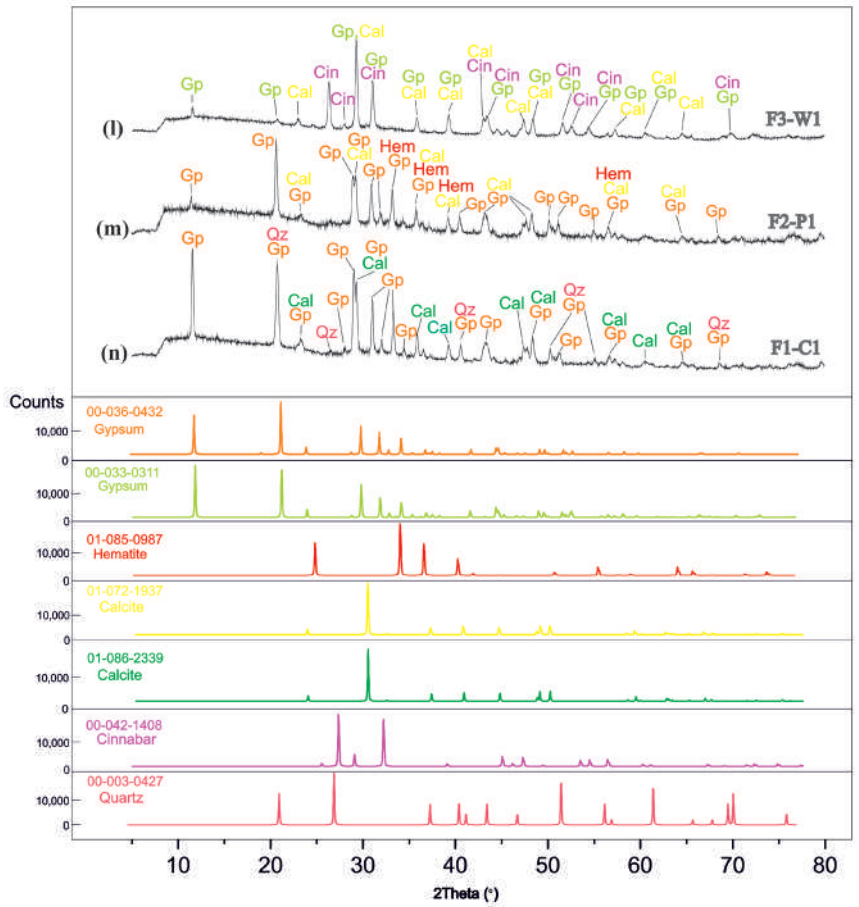

Figure 7. μ-X-ray diffraction pattern of the white, pink, and yellow samples' surface. Identified minerals: calcite (Cal), gypsum (Gp), hematite (Hem), cinnabar (Cin), quartz (Qz).

observed in red mineral based natural pigments because of the hydration of iron oxides by contact with moisture. The F4-R4 sample was shown to contain mostly calcite and hematite, while no gypsum is present. In most of samples, gypsum and calcite act as filling material, and the presence of aluminum and silicon in the samples can be connected to the presence of feldspars, clay minerals (e.g., kaolinite) and quartz in the base-material of the studied fragments. Characteristic Raman bands of hematite were observed at 226, 293, 411 and 615 cm^{-1}, 222, 290, 406, 608, and 1303 cm^{-1} and 226, 293, 411, and 612 cm^{-1}, in the spectra of F1-R1, F2-R2, and F4-R4, respectively (see Figure 8a) (Liu et al., 2022). Raman bands ascribable to gypsum were observed at 499 and 1006 cm^{-1}, and 496 and 1007 cm^{-1} in samples F1-R1 and F2-R2 (Liu et al., 2022), respectively, while characteristic Raman bands of cinnabar were observed at 253, 286, and 343 cm^{-1} in the spectrum of F3-R3 (Argote et al., 2020). The low intensity band at 551 cm^{-1}, present in the spectrum of this sample, has been assigned to goethite (Bakiler et al., 2016) which probably present in hematite as contamination. In the Raman spectrum of the F4-R4 sample, besides the bands of hematite, bands at 158, 709, and 1085 cm^{-1} were also observed, which were ascribed to calcite (Akyuz et al., 2015). In the FTIR spectra of the red samples, bands due to hematite and kaolinite (probably from the base material) were observed. The infrared spectra of hematite and kaolinite are in fact very similar, exhibiting characteristic peaks at 1032, 1008, 913, and 536 cm^{-1} (Figure 8b) (Bikiaris et al., 2000). The sharp IR band at 1398 cm^{-1} and the small peaks at 871 and 712 cm^{-1} are ascribable to calcite (Ospitali et al., 2008).

4.2. Black samples

Like the red colored fragments, the black colored F1-B1 and F2-B2 samples are characterized by high amounts of calcium and sulfur, with silicon and aluminum also present in considerable amounts. The origin of these elements is the same as indicated above for the red samples. The sample F5-B3 shows only a little amount of sulfur, revealing that

Table 3. Raman bands of minerals (or mineral based natural pigments) identified in wall paintings.

Chemical formula	Mineral/ pigment	Raman bands (cm^{-1}) and their relative intensity in qualitative terms	Ref.
$CaCO_3$	Calcite	155, 281, 712, 1086(s) 155(m), 281(m), 7128(w), 959, 1084, 1086(s), 1432, 1435, 1746	(Fikri et al., 2022) (Liu et al., 2022)
$CaSO_4 2H_2O$	Gypsum	414(m), 494(m), 669(m), 1008(s), 1137(m) 423, 500(m), 1009(s), 1134(m)	(Fikri et al., 2022) ((de Moura et al., 2023)
$Fe_{2O}3$	Hematite	220(m), 288(s), 405(m) 224(m), 290(s), 408(m), 493(w), 610(m) 225(m), 292(s), 411, 612(m), 1102, 1318	(Fikri et al., 2022) (Liu et al., 2022) (Buzgar et al., 2009)
$FeO(OH).nH_2O$	Limonite	303(w), 394(s), 562(m) 305(w), 395(s), 557(m)	(de Moura et al., 2023) (Mahmoud, 2014)
HgS	Cinnabar	253(s), 285(w), 343(m), 351(w)	(Liu et al., 2022)
C	Carbon	1383, 1578	(Mahmoud, 2014)
$K(Mg,Fe^{2+})(Fe^{3+},Al)[Si_4O_{10}](OH)_2$	Celadonite	175, 200, 277(s)	(Perez-Rodriguez et al., 2015)

Relative intensity: s, strong; w, weak; m, medium.

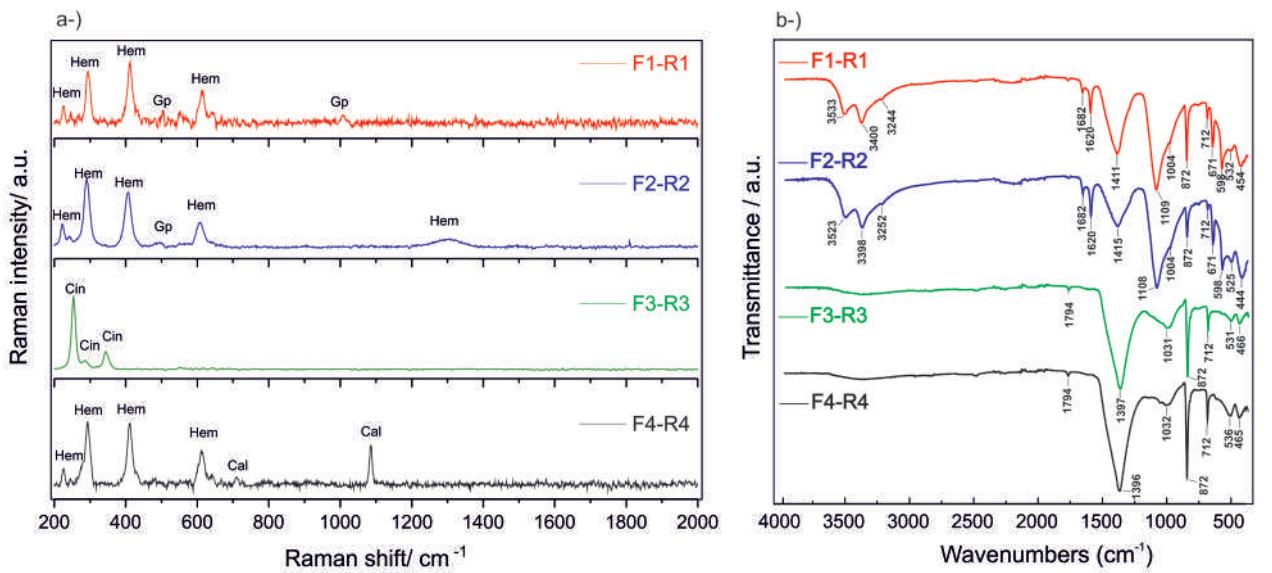

Figure 8. a) Raman and b) FTIR spectra of red samples.

gypsum is absent in this piece (a result confirmed by the XRD analysis of this sample; see Figure 5). The identified aluminum and silicon have the same origin as in the red samples. All these minerals are constituents of the base material of the samples.

The black color in all F1-B1, F2-B2, and F5-B3 samples is due to the presence of black carbon, as testified by the observation of the characteristic Raman bands of this material at ~1378 and 1580 cm^{-1} (Figure 9a) (Cerrato et al., 2021) The obtained FTIR spectra of the black colored regions are given in Figure 9b, showing the major bands of the identified base materials. On the other hand, the main characteristic band of the carbon black mineral based natural pigment, at approximately 1580 cm^{-1} (aromatic C=C stretching vibrations), could not be observed in the infrared spectra. However, the band observed at

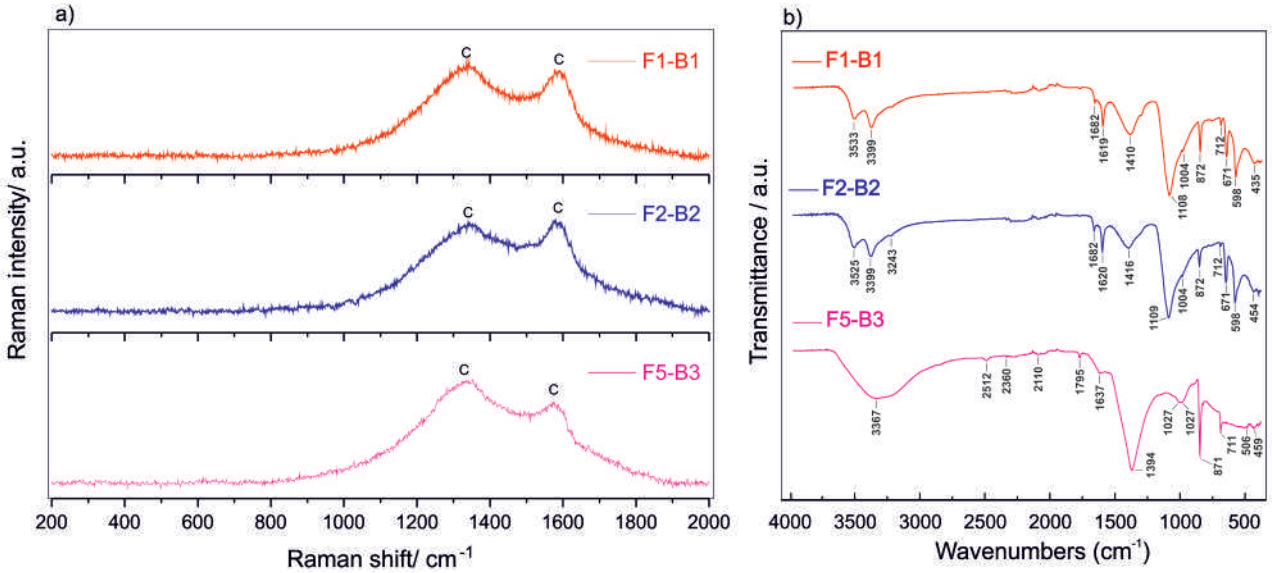

Figure 9. a) Raman and b) FTIR spectra of black samples.

approximately 1620 cm^{-1} (olefinic C=C bond stretching) undoubtedly indicates the presence of carbon in the samples.

4.3. Green and yellow samples

When compared with the red and black colored samples, the green and yellow samples share similar base materials, with gypsum and calcite dominating. Quartz, feldspars, and clay materials are also present, as testified by the results of the SEM-EDX analyses, which revealed major amounts of calcium, sulfur (higher amounts in the green samples), silicon (higher amounts in the yellow samples), and aluminum.

The presence of potassium in the green samples (F1-G1 and F2-G2) is consistent with the XRD detection of celadonite ($K(Mg,Fe^{2+})(Fe^{3+},Al)[Si_4O_{10}](OH)_2$) (Figure 6), which is responsible by the green color exhibited by the samples. In the literature, the d(060) value has been used as an indicator to distinguish celadonite from glauconite minerals using XRD (Ospitali et al., 2008; Hradil et al., 2011). In the present study, as d(060) is less than 1.51 nm in the diffractogram of all green samples (Figures 6h–6i), the presence of celadonite was confirmed. The nature of the green mineral based natural pigment has also been confirmed by the Raman analyses, where characteristic bands of celadonite could be observed: in F1-G1 (Figure 10), at 189, 273, and 550 cm^{-1}, and in F2-G2 at 199, 280, and 533 cm^{-1} (Ospitali et al., 2008; Moretto et al., 2011). In the Raman spectra of the green sample's bands due to the base materials (calcite and gypsum, in particular) were also observed (see Figure 10a). In the yellow samples, F3-Y1 and F6-Y2, calcite and gypsum were also identified by the XRD analyses, which also revealed presence of limonite in both samples and a minor amount of hematite in the F3-Y1 sample. In fact, this mineral can be defined as limonite mineral, which is the aqueous phase of goethite. In XRD analysis, the database corresponds to the mineral as goethite. These two minerals are responsible by the different yellow tones of the two samples, with F3-Y1 showing a more orange-like coloration (see Figure 3) due to the presence of the red hematite mineral based natural pigment. Both the Raman and FTIR measurements confirm the presence of limonite as the mineral based natural pigment giving the yellow color to the pieces, with the characteristic Raman bands of this mineral being observed at ca. 549 and 552 cm^{-1} (Figure 10a), and the infrared mark bands being observed at 1029 and 1006 cm^{-1} (comparing well with the literature values of 1032 cm^{-1} and 1004 cm^{-1}) (Bakiler et al., 2016).

4.4. White, pink, and cream samples

As the remaining samples, the studied fragments exhibiting white pink and cream colors have major amounts of calcium and sulfur, and significant amounts of silicon and aluminum, which reflect the constitution of their base material. These SEM-EDX results were fully confirmed by the XRD, Raman and FTIR data, where calcite and gypsum were identified as main minerals present in the samples (Figure 7 and Figure 11). The amount of calcite is particularly large in the white sample, F3-W1, since in this case the mineral acts also as mineral based natural pigment. This sample was taken from the same fragment as F3-R3 (see Figure 3), where cinnabar was identified, and red spots are also observed in the F3-W1 sample. The XRD analysis of the piece thus reveals presence of cinnabar together with the calcite and gypsum (Figure 7).

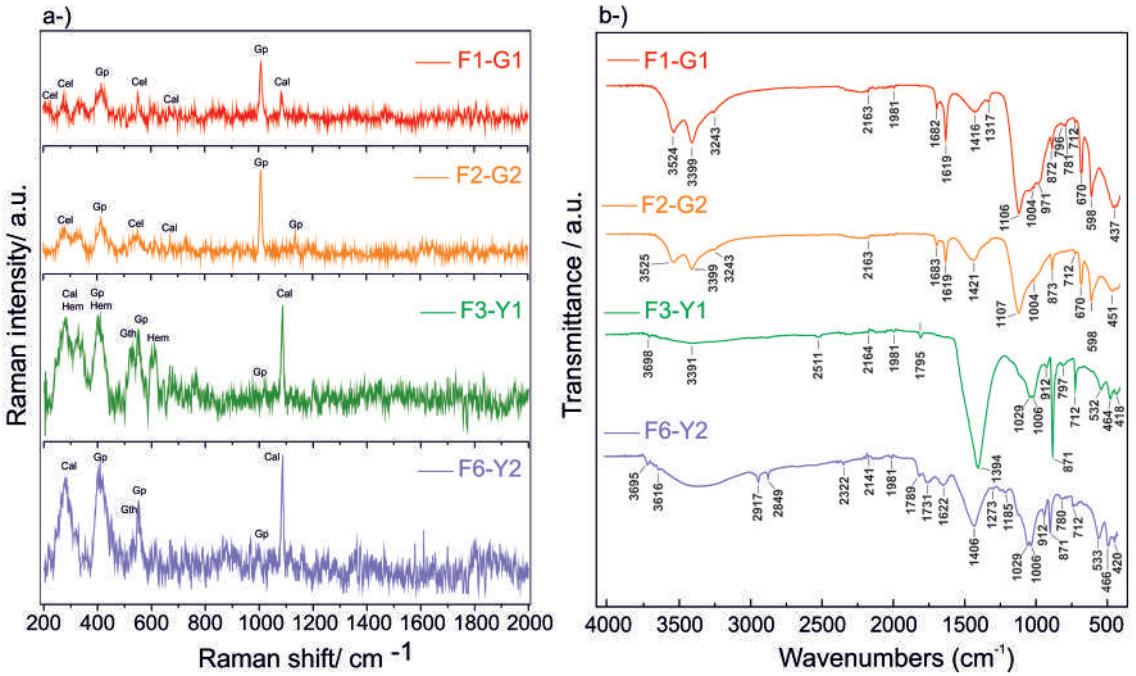

Figure 10. a) and FTIR b) spectra of green and yellow samples.

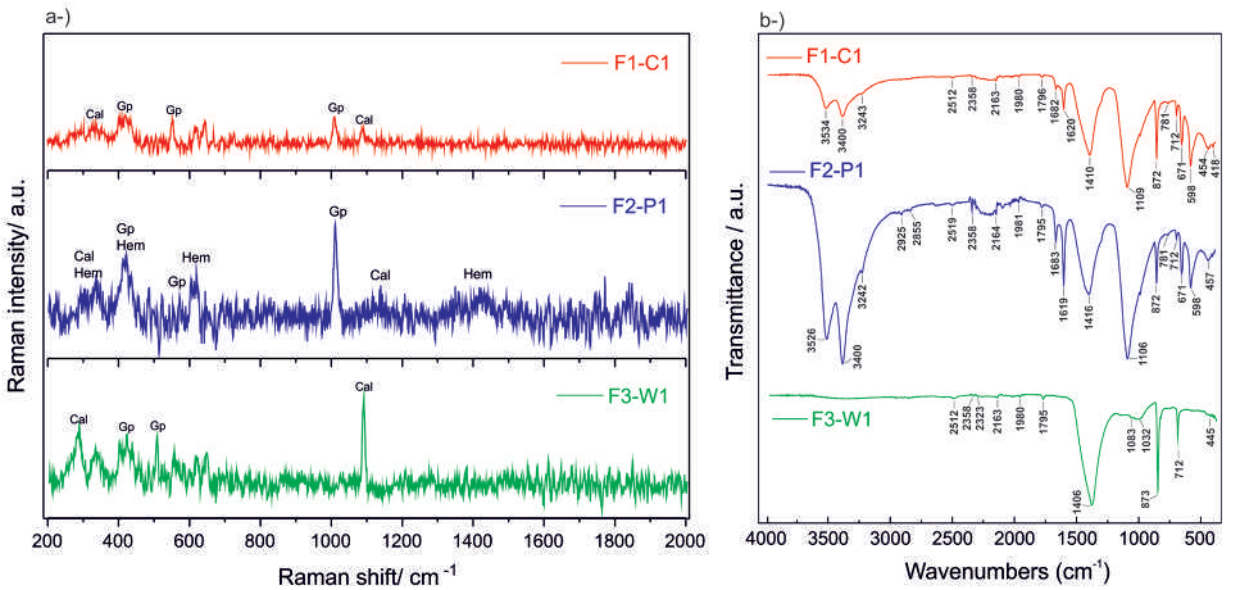

Figure 11. a) FTIR, b) Spectra of cream, pink, and white samples.

The pink color of sample F2-P1 is due to hematite, which has been identified in this sample by both XRD and Raman spectroscopy (see Figure 7 and Figure 11a), while, accordingly, the SEM-EDX results show the presence of a significant amount of iron in this sample.

Finally, the cream colored F1-C1 sample owns its color most probably to trace amounts of iron oxides (hematite and limonite most probably), but these minerals could not be detected in the performed XRD and spectroscopic measurements. Nevertheless, the SEM-EDX analysis shows that a small amount of iron is indeed present in the F1-C1 sample.

The obtained results are summarized in Table 4. Two red mineral based natural pigments were identified in

Table 4. Summary of the results obtained with the different analytical methods.

Colour	Sample	Elements detected by SEM-EDX	Minerals detected by XRD	Raman bands (cm^{-1})	FTIR (cm^{-1})
Red	F1-R1	Ca, S, Si, Fe, Al, Na, Mg	Calcite	280, 711	712, 872, 1793
			Gypsum	414, 494, 1008	598, 671, 1004, 1109, 1620, 1682, 3244, 3400, 3533
			Hematite	224, 290, 408, 493, 616	532, 454
	F2-R2	Ca, S, Fe, Si, Al, Mg, Na	Calcite	710	712, 872, 1795
			Gypsum	413, 494, 1009	598, 671, 1004, 1108, 1682, 3252, 3398, 3523
			Hematite	223, 292, 615, 1308	525, 444
	F3-R3	Ca, Hg, S, Si, Al, Fe, Na	Calcite	nd	712, 872, 1794
			Gypsum, Goethite	nd	nd
			Hematite	291, 616	531, 466, 1397
			Cinnabar	254, 285, 344	712, 1031
	F4-R4	Ca, Si, Fe, Al, Mg	Calcite	712, 1087	712, 872, 1794
			Gypsum	nd	nd
			Hematite	227, 293, 410, 612	536, 465
Black	F1-B1	S, Ca, Si, Al	Calcite	1378*, 1580*	712, 872
			Gypsum	nd	598, 671, 1004, 1108, 1619, 1682, 3399, 3533
			Quartz	nd	nd
	F2-B2	Ca, S, Si, Al, Mg, Fe, Na	Calcite	1377*, 1578*	712, 872
			Gypsum		598, 671, 1004, 1109, 1620, 1682, 3399, 3525
	F5-B3	Ca, Si, Al, Mg, Na	Calcite	1380*, 1580*	711, 871, 1795
Green	F1-G1	Ca, S, Si, Fe, Al, K	Calcite	709, 1083	712, 872
			Gypsum	415, 1007	598, 670, 1004, 1106, 1416, 1619, 1682, 3243, 3399, 3524
			Celadonite	189, 273, 550	437, 796, 971
	F2-G2	Ca, S, Si, Al, Fe, K	Calcite	710	712, 873
			Gypsum	414, 1006, 1136	598, 670, 1004, 1107, 1421, 1619, 1683, 3243, 3399, 3525
			Celadonite	199, 280, 533	nd

Table 4. (Continued)

Yellow	F3-Y1	Ca, Si, S, Al, Fe, Mg	Calcite	155, 1085, 1087	712, 871, 1795, 2511
			Hematite	284, 287, 609	464, 532, 1029
			Limonite	549, 552	797
	F6-Y2	Ca, Si, Al, Fe	Calcite	156, 1086, 1088	712, 871, 1406, 1789
			Gypsum	408, 414	466, 1006, 2322
			Limonite	549, 553	780, 1622
Cream	F1-C1	Ca, S, Si, Al	Calcite	155, 273, 1083	712, 872, 1796, 2512
			Gypsum	415, 528, 1007	598, 671, 1109, 1620, 1682, 3243, 3400, 3534
			Quartz	-	nd
Pink	F2-P1	Ca, S, Si, Al, Mg, Fe, Na	Calcite	281, 1085	712, 872, 1795, 2519
			Gypsum	416, 529, 1007	598, 671, 1106, 1619, 1683, 3242, 3400, 3526
			Hematite	227, 1067, 1346	457
White	F3-W1	Ca, Si, S, Al, Fe	Calcite	285, 1087	712, 873, 1795, 2512
			Gypsum	418, 526	nd
			Cinnabar	-	712, 1032

nd: not detected, * characteristic bands of carbon black.

the studied frescoes paintings: hematite (present in most of the samples) and cinnabar. The black-colored areas derive their color from the presence of amorphous carbon (carbon black), while celadonite was identified as the green mineral based natural pigment. The yellow color is believed to be achieved by mixing hematite and limonite with the base mineral's gypsum and calcite. In the XRD measurements conducted on the white-colored fragment, the presence of the red cinnabar mineral based natural pigment was detected (along with gypsum and calcite). In the white region, the sample exhibits visible red spots, which could be attributed to either the application of white (calcite-based) paint over a red (cinnabar-based) layer or the addition of a very small amount of cinnabar to the white paint. This investigation emphasizes the importance of employing a multi-analytic approach for characterizing the historical wall fresco paints, particularly in identifying the mineral based natural pigments used. The SEM-EDX analyses of the samples yielded crucial data concerning the chemical element contents in each studied sample, facilitating the interpretation of both XRD and spectroscopic (Raman and FTIR) data.

Table 5 presents a comparative examination of techniques used for the analysis and mineral based natural pigment detection in historical wall paintings from various locations.

5. Conclusion

In conclusion, the characterization of different mineral based natural pigments used in the walls of Atik Mustafa Pasha Mosque from the Byzantine period has been extensively investigated using various techniques. These advanced techniques have provided valuable insights into the chemical composition of mineral based natural pigments, identification of chemical functional groups, and understanding crystal structures, contributing significantly to art historical studies. This study revealed the presence of two distinct red mineral based natural pigments in the examined fresco paintings: hematite, prevalent in most samples, and cinnabar. Black-colored areas derive their color from the presence of amorphous carbon (carbon black), while celadonite has been identified as the green mineral based natural pigment. The yellow color is believed to result from a mixture of hematite and limonite with the base minerals gypsum and calcite, which probably come from intonaco of wall paintings. XRD measurements on the white-colored fragment detected the presence of the red cinnabar mineral based natural pigment along with gypsum and calcite. This study emphasizes the importance of a multi-analytic approach in characterizing historical wall paintings, particularly in identifying the mineral based natural mineral based pigments used. Additionally, the SEM-EDX analyses revealed how the

Table 5. Comparative examination of techniques for analysis and mineral based natural pigment detection in historical wall paintings from various locations.

Region/ Country	Technique	Results	Time	References
Morocco	XRF, Raman, ATR-FTIR	Hematite, cinnabar, gypsum calcite, carbon black.	9^{th}–12^{th} century	(Fikri et al., 2022)
Sinop, Türkiye	XRF, Raman, ATR-FTIR	Calcite, red ochre, goethite, cinnabar, green earth, carbon black.	2^{nd}–4^{th} cent. A.D. Late roman period	(Bakiler et al., 2016)
Isfahan, Iran	SEM-EDS, micro Raman, FTIR,	Ultramarine.	17^{th}–4^{th} century	(Koochakzaei et al., 2022)
Tuscany, Italy	SEM-EDS, micro Raman, XRF	Ferroceladonite, hematite, gypsum, calcite, goethite.	14^{th} century	(Marrocchino et al., 2022)
Mani Peninsula, Greece	SEM, FTIR, XRD, XRF	Hematite, powdered charcoal, cinnabar, minium, ultramarine blue, celadonite or glauconite.	10^{th}–15^{th} century	(Hein et al., 2009)
İstanbul, Türkiye	SEM-EDS, XRD, FTIR, and micro Raman	Hematite, cinnabar, limonite, calcite, gypsum, celadonite	9^{th} century	In this study

XRD, Raman, and FTIR data complement each other in illuminating the historical details of wall paints, similar to findings in studies conducted in the global literature. Future studies will have the opportunity to delve deeper into earlier periods through the integration of surface analysis, chemical characterization, and image processing-artificial intelligence algorithms.

References

Akyol AA, Demirci S, Kadioglu YK, Turkmenoglu AG (2005). Conservation res-tauration et Analyses Techniques Analyse Preliminaire des Materiaux des Espaces P9 (a6) et P26 (C13) du Secteur A (Chantier 12). In Zeugma II Peintures Murales Romaines Varia Anatolica 27: 248–268.

Akyol AA, Kadıoğlu YK, Demirci Ş (2011). Zeugma (Gaziantep) Antik Kenti Du-var Resimleri Arkeometrik Çalışmaları. Anadolu University Journal of Science and Technology A - Applied Sciences and Engineering 12: 37–56.

Akyuz S, Akyuz T, Basaran S, Kocabas I, Gulec A et al. (2009). FT-IR and EDXRF analysis of wall paintings of ancient Ainos Hagia Sophia Church. Journal of Molecular Structure 924–926: 400–403. https://doi.org/10.1016/j.molstruc.2009.01.020

Akyuz T, Akyuz S, Gulec A (2015). Elemental and spectroscopic characterization of plasters from Fatih Mosque-Istanbul (Turkey) by combined micro-Raman, FTIR and EDXRF techniques. Spectrochimica Acta Part A: Molecular and Biomolecular Spectroscopy 149: 744–750. https://doi.org/10.1016/j.saa.2015.05.015

Argote DL, Torres G, Hernández-Padrón G, Ortega V, López-García PA et al. (2020). Cinnabar, hematite and gypsum presence in mural paintings in Teotihuacan, Mexico. Journal of Archaeological Science: Reports 32: 1-15. https://doi.org/10.1016/j.jasrep.2020.102375

Bakiler M, Kırmızı B, Ormancı Ö, Hanyalı Ö, Dağ, E et al. (2016). Material characterization of the Late Roman wall painting samples from Sinop Balatlar Church Complex in the black sea region of Turkey. Microchemical Journal 126: 263–273. https://doi.org/10.1016/j.microc.2015.11.050

Barone G, Mazzoleni P, Cecchini A, Russo A (2018). In situ Raman and pXRF spectroscopic study on the wall paintings of Etruscan Tarquinia tombs. Dyes and Pigments 150: 390–403. https://doi.org/10.1016/j.dyepig.2017.12.008

Bell IM, Clark RJH, Gibbs PJ (1997). Raman spectroscopic library of natural and synthetic pigments (pre- ≈ 1850 AD). Spectrochimica Acta Part A: Molecular and Biomolecular Spectroscopy 53: 2159–2179. https://doi.org/10.1016/s1386-1425(97)00140-6

Bikiaris D, Daniilia S, Sotiropoulou S, Katsimbiri O, Pavlidou E et al. (2000). Ochre-differentiation through micro-Raman and micro-FTIR spectroscopies: application on wall paintings at Meteora and Mount Athos, Greece. Spectrochimica Acta Part A: Molecular and Biomolecular Spectroscopy 56: 3–18. https://doi.org/10.1016/s1386-1425(99)00134-1

Buzgar N, A I Apopei, A Buzatu (2009). Romanian database of Raman spectroscopy.

Cerrato EJ, Cosano D, Esquivel D, Jiménez-Sanchidrián C., Ruiz JR (2021). Spectroscopic analysis of pigments in a wall painting from a high Roman Empire building in Córdoba (Spain) and identification of the application technique. Microchemical Journal 168: 106444. https://doi.org/10.1016/j.microc.2021.106444

Crupi V, Galli G, la Russa MF, Longo F, Maisano G et al. (2015). Multi-technique investigation of Roman decorated plasters from Villa dei Quintili (Rome, Italy). Applied Surface Science 349: 924–930. https://doi.org/10.1016/j.apsusc.2015.05.074

de Moura J, Lage MC, Farias Filho B, de Faria DL, de Barros W et al. (2023). Multi-Analytical Characterization of Rupestrian Precolonial Paintings of Inhuma, Piauí, Brazil. Journal of Brasilian Chemical Society. 34 (6): 826-837. https://doi.org/10.21577/0103-5053.20220151

Demus O (1964). Byzantine Mosaic Decoraiton - Aspects of Monumental Art in By-zantium. Boston Book and Art Shop, Boston.

Dooryhée E, Anne M, Bardiès I, Hodeau JL, Martinetto P et al. (2005). Non-destructive synchrotron X-ray diffraction mapping of a Roman painting. Applied Physics A 81: 663–667. https://doi.org/10.1007/s00339-005-3281-6

Edwards HGM, Newton EM, Russ J (2000). Raman spectroscopic analysis of pigments and substrata in prehistoric rock art. Journal of Molecular Structure 550–551: 245–256. https://doi.org/10.1016/s0022-2860(00)00389-6

Encyclopedia of the Hellenic World, (2023).

Esmer M (2016). Critisism of Unsustainability at Ayvansaray as an Urban Archaeolo-gical Site, in: International Conference on New Trends in Architecture and Inte-rior Design.

Eyice S (1991a). Atik Mustafa Paşa Camii. TDV İslam Ansiklopedisi (in Turkish).

Eyice S (1991b). Ayvansaray. TDV İslam Ansiklopedisi (in Turkish).

Fikri I El, Amraoui M, Haddad M, Ettahiri AS, Falguères C et al. (2022). Raman and ATR-FTIR analyses of medieval wall paintings from al-Qarawiyyin in Fez (Morocco). Spectrochimica Acta Part A: Molecular and Biomolecular Spectroscopy 280: 121557. https://doi.org/10.1016/j.saa.2022.121557

Franquelo ML, Duran A, Herrera LK, Jimenez de Haro MC, Perez-Rodriguez JL (2009). Comparison between micro-Raman and micro-FTIR spectroscopy techniques for the characterization of pigments from Southern Spain Cultural Heritage," Journal of Molecular Structure 924–926: 404–412, https://doi.org/10.1016/j.molstruc.2008.11.041

Germinario C, Francesco I, Mercurio M, Langella A, Sali D et al. (2018). Multi-analytical and non-invasive characterization of the polychromy of wall paintings at the Domus of Octavius Quartio in Pompeii. The European Physical Journal Plus 133: 359. https://doi.org/10.1140/epjp/i2018-12224-6

Gilbert B, Denoël S, Weber G, Allart D (2003). Analysis of green copper pigments in illuminated manuscripts by micro-Raman spectroscopy," Analyst 128 (10): 1213–1217. https://doi.org/10.1039/B306138H

Hein A, Karatasios I, Mourelatos D (2009). Byzantine wall paintings from Mani (Greece): microanalytical investigation of pigments and plasters. Analytical an Bioanalytical Chemistry 395: 2061–2071. https://doi.org/10.1007/s00216-009-2967-6

Hradil D, Píšková A, Hradilová J, Bezdička P, Lehrberger G et al. (2011). Mineralogy of bohemian green earth pigment and its microanalytical evidence in historical paintings. Archaeometry 53: 563–586. https://doi.org/10.1111/j.1475-4754.2010.00554.x

Kızılkayak G (2023) GABAM, Koç University.

Koochakzaei A, Hamzavi Y, Mousavi M al-SS (2022). Characterization of the mural blue paintings in ornamental motif of Ali Qapu palace in Isfahan, Iran, using spectroscopic and microscopic methods (a case study). Journal of Archaeological Science: Reports 45: 103632. https://doi.org/10.1016/j.jasrep.2022.103632

Liu Z, Yang R, Wang W, Xu W, Zhang M (2022). Multi-analytical approach to the mural painting from an ancient tomb of Ming Dynasty in Jiyuan, China: Characterization of materials and techniques. Spectrochimica Acta Part A: Molecular and Biomolecular Spectroscopy 279: 121419. https://doi.org/10.1016/j.saa.2022.121419

Mahmoud HHM (2014). Investigations by Raman microscopy, ESEM and FTIR-ATR of wall paintings from Qasr el-Ghuieta temple, Kharga Oasis, Egypt. Heritage Science 2: 18. https://doi.org/10.1186/s40494-014-0018-x

Marrocchino E, Telloli C, Grazia Paletta M, Leis M, Vaccaro C (2022). The mu-ral paintings of the cloister in the Certosa di Calci, Pisa. Journal of Archaeological Science: Reports 43: 103461. https://doi.org/10.1016/j.jasrep.2022.103461

Mathews TF, Ernest JWH (1985). Notes on the Atik Mustafa Paşa Camii in Istanbul and Its Frescoes. Dumbarton Oaks Papers 39: 125–134. https://doi.org/10.2307/1291520

Mazzocchin GA, Agnoli F, Salvadori M (2004). Analysis of Roman age wall paintings found in Pordenone, Trieste and Montegrotto. Talanta 64: 732–741. https://doi.org/10.1016/j.talanta.2004.03.055

Moretto LM, Orsega EF, Mazzocchin GA (2011). Spectroscopic methods for the analysis of celadonite and glauconite in Roman green wall paintings. Journal of Cultural Heritage 12: 384–391. https://doi.org/10.1016/j.culher.2011.04.003

Olin JS (1966). The use of infrared spectrophotometry in the examination of pain-tings and ancient artifacts. Instrument News 17: 1–4.

Ospitali F, Bersani D, Di Lonardo G, Lottici PP (2008). 'Green earths': vibratio-nal and elemental characterization of glauconites, celadonites and historical pigments. Journal of Raman Spectroscopy 39: 1066–1073. https://doi.org/10.1002/jrs.1983

Perez-Rodriguez JL, de Haro M del CJ, Siguenza B, Martinez-Blanes JM (2015). Green pigments of Roman mural paintings from Seville Alcazar. Applied Clay Science 116–117: 211–219. https://doi.org/10.1016/j.clay.2015.03.016

Piovesan R, Maritan L, Amatucci M, Nodari L, Neguer J (2016). Wall painting pigments of Roman Empire age from Syria Palestina province (Israel). European Journal of Mineralogy 28: 435–448. https://doi.org/10.1127/ejm/2015/0027-2500

Rosado T, Martins MR, Pires M, Mirão J, Candeias A et al. (2013). Enzymatic monitorization of mural paintings biodegradation and biodeterioration. International Journal of Conservation Science 4: 603–612.

Smith GD, Clark RJH (2004). Raman microscopy in archaeological science. Journal of Archaeological Science 31: 1137–1160. https://doi.org/10.1016/j.jas.2004.02.008

Tomasini EP, Halac EB, Reinoso M, Di Liscia EJ, Maier MS (2012). Micro-Raman spectroscopy of carbon-based black pigments. Journal of Raman Spectroscopy 43: 1671–1675. https://doi.org/10.1002/jrs.4159

Türkyılmaz F (2023). Atik Mustafa Paşa Camii'ndeki restorasyon tarihe ışık tutuyor (in Turkish).

Uvarov V, Popov I, Rozenberg S (2015). X-ray Diffraction and SEM Investigation of Wall Paintings Found in the Roman Temple Complex at Horvat Omrit, Israel. Archaeometry 57: 773–787. https://doi.org/10.1111/arcm.12124

Van 't Hul-Ehrnreich, EH (1970). Infrared Microspectroscopy for the Analysis of Old Painting Materials. Studies in Conservation 15: 175. https://doi.org/10.2307/1505580

Weber J, Prochaska W, Zimmermann N (2009). Microscopic techniques to study Roman renders and mural paintings from various sites. Materials Characterization 60: 586–593. https://doi.org/10.1016/j.matchar.2008.12.008

Wiener Müller-Wolfgang (2001). İstanbul'un tarihsel topoğrafyası. Yapı Kredi Yayın-ları, İstanbul (in Turkish).

Zeng QG, Zhang GX, Leung CW, Zuo J (2010). Studies of wall painting frag-ments from Kaiping Diaolou by SEM/EDX, micro-Raman and FT-IR spectroscopy. Microchemical Journal 96: 330–336. https://doi.org/10.1016/j.microc.2010.05.013

Zimmermann NLS (2011). Wall painting in Ephesos from the Hellenistic to the By-zantine period.